Electronic Supplementary Information

Quantitative Assessment of the Carbocation/Carbene Character of the Gold-Carbene Bond

Keith M. Azzopardi,[a,†] *Giovanni Bistoni,*[b,c,†] *Gianluca Ciancaleoni,*[b,*] *Francesco Tarantelli,*[b,c] *Daniele Zuccaccia,*[b,d] *Leonardo Belpassi*[b,*]

[a] Metamaterials Unit, Faculty of Science, University of Malta, Msida, MSD 2080, Malta

[b] Istituto di Scienze e Tecnologie Molecolari del CNR (CNR-ISTM), c/o Dipartimento di Chimica, Biologia e Biotecnologie, Universita degli Studi di Perugia, via Elce di Sotto 8, I-06123, Perugia, Italy

[c] Dipartimento di Chimica, Biologia e Biotecnologie, Universita degli Studi di Perugia, via Elce di Sotto 8, I-06123, Perugia, Italy

[d] Dipartimento di Chimica, Fisica e Ambiente, Università di Udine, Via Cotonificio 108, I-33100 Udine, Italy

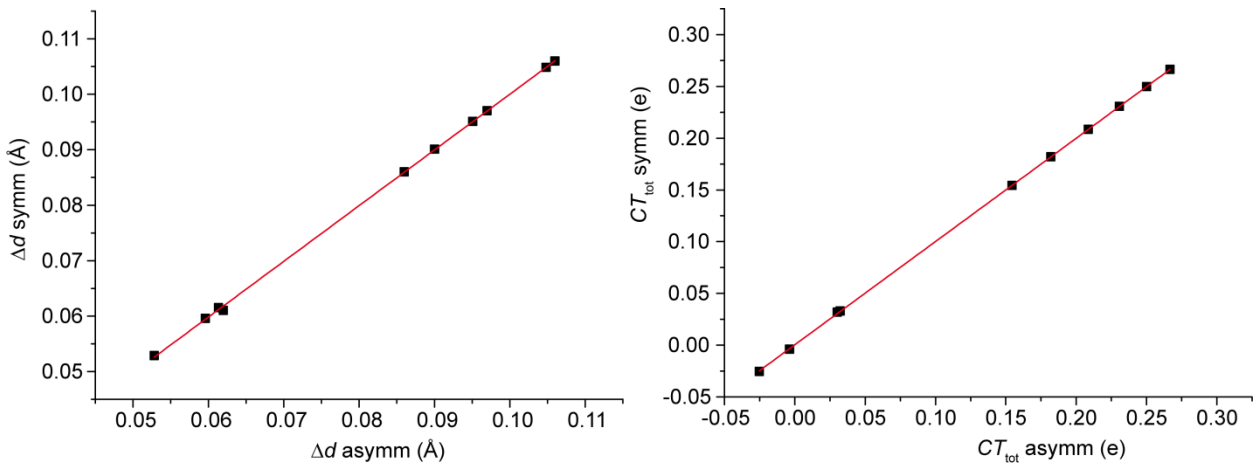

Figure S1. Correlation between Δd and CT_{tot} for unconstrained (asymm) and C_s-constrained geometries (symm) of [LAu-**S**]$^{n+}$.

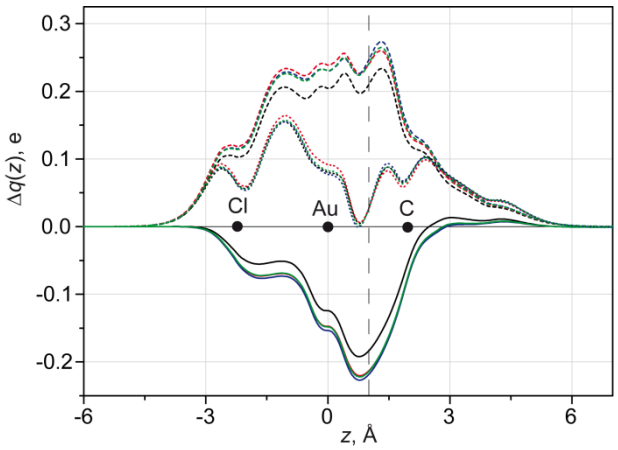

Figure S2a. Symmetry-separated Charge Displacement Functions for [ClAu**S**] calculated with different exchange-correlation functional approximations. The black dots represent the *z* coordinate of the atoms. The dotted vertical line identifies a suitable boundary between the fragments. Solid lines are related to the A'' symmetry (back-donation), dashed lines to the A' symmetry (donation) and dotted lines to the total. Black, red, blue and green lines are calculated using the B3LYP, BLYP, LDA and BP86 functional, respectively. Back-donation values are 0.182, 0.212, 0.217 and 0.212 e for B3LYP, BLYP, LDA and BP86 functional, respectively. Donation values are 0.212, 0.242, 0.249 and 0.244 e for B3LYP, BLYP, LDA and BP86 functional, respectively.

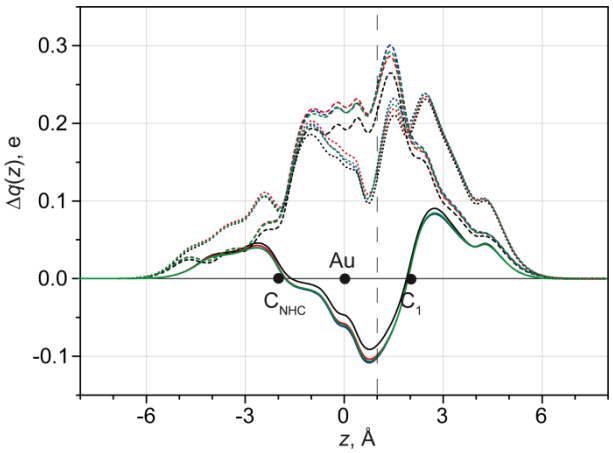

Figure S2b. Symmetry-separated Charge Displacement Functions for [**NHC**Au**S**] calculated with different exchange-correlation functional approximations. The black dots represent the *z* coordinate of the atoms. The dotted vertical line identifies a suitable boundary between the fragments. Solid lines are related to the A'' symmetry (back-donation), dashed lines to the A' symmetry (donation) and dotted lines to the total. Black, red, blue and green lines are calculated using the B3LYP, BLYP, LDA and BP86 functional, respectively. Back-donation values are 0.084, 0.097, 0.101 and 0.098 e for B3LYP, BLYP, LDA and BP86 functional, respectively. Donation values are 0.219, 0.244, 0.252 and 0.252 e for B3LYP, BLYP, LDA and BP86 functional, respectively.

As it can be seen in Figure S2a and S2b, the BLYP, BP86 and LDA functionals give essentially the same results in the computation of the DCD components of the Au-C1 bond. The inclusion of the exact exchange in the functional definition (the B3LYP case) tends to reduce slightly both components (about 14% and 13% for the back-donation and donation, respectively). It is interesting to note that since these differences compensate each other, the resulting total CDF (computed by B3LYP) is almost identical to the CDFs computed with the other functionals. The difference between B3LYP and other functionals is expected to be quite systematic (same percentage is found for neutral and cationic complexes) and it is not expected to alter the trend of the ligands.

Table S1. Geometrical parameters (in Å) of **S**, Au-C_1 electronic components (in electrons), rotational barrier of the C_1C_2 bond ($\Delta^{\ddagger}E_r$, in kcal/mol) and P_{back} (%) for the different [LAu-**S**]$^{+/0}$ complexes.

L	d_{C1C2}	d_{C2C3}	d_{C3C4}	Δd	CT_{tot}	CT_{don}	CT_{back}	$\Delta^{\ddagger}E_r$	P_{back}
CH_3O^-	1.467	1.538	1.485	0.053	-0.025	0.268	-0.293	5.6	52
F^-	1.462	1.541	1.482	0.059	-0.004	0.237	-0.241	6.1	46
Cl^-	1.461	1.542	1.481	0.061	0.032	0.244	-0.212	6.2	45
Ph$^-$	1.460	1.542	1.480	0.062	0.033	0.229	-0.196	6.3	44
PF_3	1.434	1.567	1.463	0.104	0.266	0.317	-0.051	9.7	5
PH_3	1.439	1.563	1.466	0.097	0.231	0.299	-0.068	9.2	12
PMe_3	1.443	1.559	1.468	0.091	0.203	0.277	-0.074	8.9	17
NHC	1.445	1.556	1.470	0.086	0.154	0.252	-0.098	8.4	22
CO	1.433	1.568	1.462	0.106	0.250	0.298	-0.048	9.9	4
Py	1.442	1.558	1.468	0.090	0.182	0.298	-0.116	8.3	18
PB	1.439	1.561	1.466	0.095	0.208	0.299	-0.091	8.8	14

[a]Average value between d_{C2C3} and d_{C2C4}.

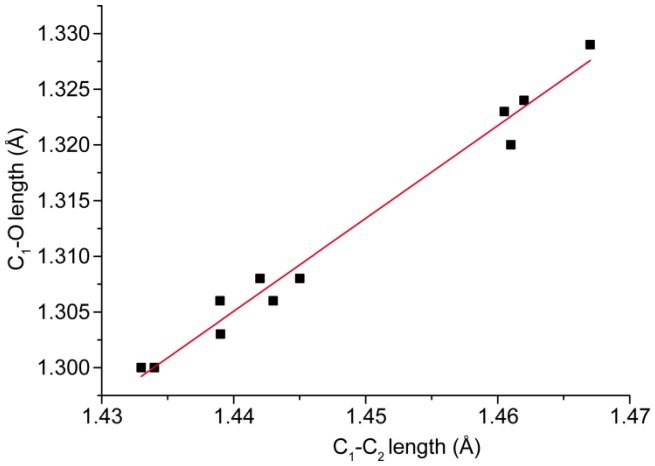

Figure S3. Linear correlation between C_1C_2 and C_1O bond length for [LAu-**S**]$^{+/0}$ complexes.

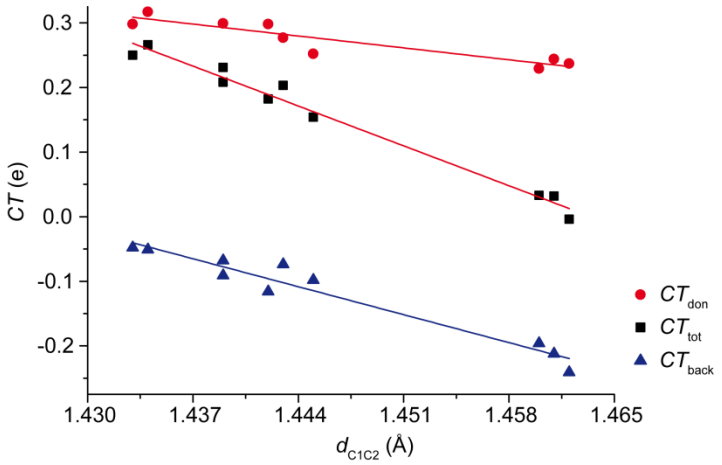

Figure S4. Linear correlations between d_{C1C2} and CT_{tot}, CT_{don} and CT_{back} for [LAu-**S**]$^{+/0}$ complexes.

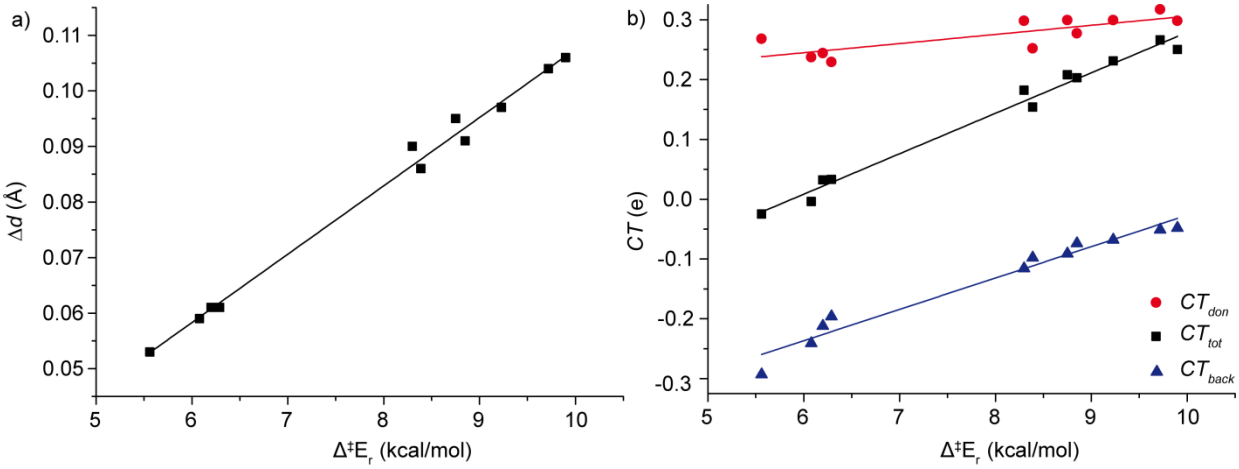

Figure S5. Panel a) Linear correlation between $\Delta^{\ddagger}E_r$ and Δd for [LAu-**S**]$^{+/0}$ complexes. Panel b) Linear correlations between $\Delta^{\ddagger}E_r$ and CT_{tot}, CT_{don} and CT_{back} for [LAu-**S**]$^{+/0}$ complexes.

Role of CT_{don} and electrostatics. Here we try to extend the scope of the methodology, considering also systems without any ligand ([Au-**S**]$^+$), different oxidation state ([Cl_3Au-**S**]) or metals ([ClAg-**S**] and [ClCu-**S**]). The aim of this study is to test the generality of the proposed method for evaluating electronic properties of the metallic fragment. In particular, by changing the metal and the oxidation state, we expect to affect also the values of CT_{don}, that was remarkably constant along the gold(I) series. Indeed, in these cases, CT_{don} varies very much, passing from 0.142 e for [ClCu-**S**]$^+$ to 0.526 for [Au-**S**]$^+$ (Table S2). In addition, we also optimized the structures of the isolated fragment (**S**), the fragment with a positive point charge (**Q**$^+$) in the position that gold occupies in [Au-**S**]$^+$ (**SQ**$^+$), and the protonated carbene (**SH**$^+$).

Table S2. Geometrical parameters (in Å) of **S**, Au-C1 electronic components (in electrons) and rotational barrier of the C_1C_2 bond ($\Delta^{\ddagger}E_r$, in kcal/mol) for complexes different than [LAu-**S**]$^{+/0}$ and in absence of any metal.

L	d_{C1C2}	d_{C2C3}	d_{C3C4}	Δd	CT_{tot}	CT_{don}	CT_{back}	$\Delta^{\ddagger}E_r$
[ClAg-**S**]$^+$	1.457	1.546	1.478	0.068	0.037	0.162	-0.125	6.7
[ClCu-**S**]$^+$	1.462	1.543	1.481	0.062	-0.044	0.142	-0.186	-
[Au-**S**]$^+$	1.431	1.567	1.464	0.102	0.424	0.526	-0.105	8.9
[Cl_3Au-**S**]$^+$	1.443	1.548	1.476	0.072	0.243	0.403	-0.161	6.2
S	1.469	1.545	1.480	0.064	-	-	0	6.7
SQ$^+$	1.417	1.572	1.457	0.115	-	-	0	-
SH$^+$	1.408	1.581	1.454	0.127	-	-	0	12.9

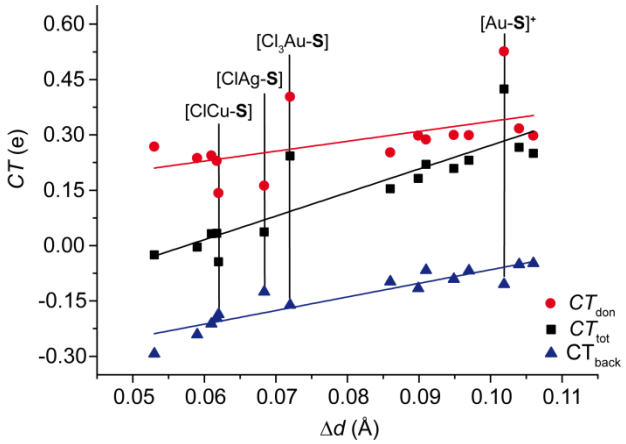

Figure S6. Linear correlations between Δd and CT_{tot}, CT_{don} and CT_{back} for all the complexes.

Plotting the different Au-C bond components *vs.* Δd for all the symmetric [L_nM-**S**]$^{n+}$ complexes, all the linear correlations are worse than in Figure 2b (see the main text) (Figure S5). In particular, a

certain correlation is still present between Δd and CT_{back} (r^2 = 0.8580), and completely absent between Δd and CT_{don} (r^2 = 0.2951). In particular, $[Au\text{-}\mathbf{S}]^+$ and $[Cl_3Au\text{-}\mathbf{S}]^+$ are dramatically different than in the case of other ligands. Consequently, also the correlation between Δd and CT_{tot} is low (r^2 = 0.7773).

In order to better understand the factors determining Δd, it is really informative the comparison of $\mathbf{SQ}^+$, $\mathbf{SH}^+$ and $\mathbf{SAu}^+$. We use $\mathbf{SQ}^+$ as a prototype for studying the pure electrostatic effect, in $\mathbf{SH}^+$ both electrostatics and donation are present, in $\mathbf{SAu}^+$ we have the concomitant presence of donation, back-donation and electrostatic effects.

The electronic structure of **S** in the presence of a positive point charge $\mathbf{Q}^+$ can be described as a combination of the limit resonance structures **R1''-3''** (Scheme S1).

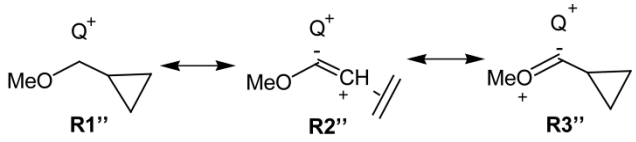

Scheme S1. Three limit resonance structures describing the complex **S** in presence of a positive point charge Q^+.

Within this model, the presence of $\mathbf{Q}^+$ shall increase the contribution of the **R2''** and **R3''** structures, thus decreasing the d_{C1C2} and d_{C3C4}, and increasing d_{C2C4} and, consequently, Δd (Table S2).

Indeed, the presence of a positive point charge close to C_1 (at the distance of 1.975 Å) dramatically influences the geometric parameters of **S** (Table S2): d_{C1C2} passes from 1.469 to 1.417 Å, whereas d_{C1O} passes from 1.325 to 1.284 Å. The shortening of these bonds is consistent with the increased bond order in **R2''** and **R3''**. Moreover C_2C_3 and C_3C_4 react differently at the presence of the point charge, the former lengthens and the latter shortens, coherently with the increasing importance of **R2''**.

Qualitatively, the electrostatic effect on the electron density rearrangement of **S** due to the presence of $\mathbf{Q}^+$ can be evaluated by computing the electronic density difference between $\mathbf{SQ}^+$ and **S**. Since **S** is C_s-symmetric, the A' and A'' contributions can also be separately analyzed. The three dimensional contour plots of $\Delta\rho$(A'') (Figure S6b) demonstrate that the point charge considerably strengthens the π component of the C_1C_2 bond, leading to a shortening of the bond. Moreover, the visual analysis of $\Delta\rho$(A') (Figure S6a) reveals that the σ component of the C_1C_2 bond is also strongly polarized by the presence of the point charge. Also the bond polarization likely contributes to modifying the length of the C_1C_2 bond.

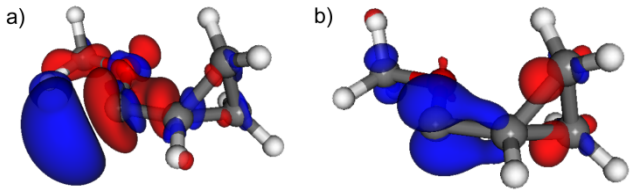

Figure S7. Three dimensional contour plots of the symmetry components of the electron density difference between **SQ**$^+$ and **S**. a) A' component. b) A'' component.

The situation in **SH**$^+$ is very similar to the one just described. In this case, both C_1C_2 and C_1O shortens, to 1.408 and 1.286 Å, respectively. These shortening are almost equal to the one observed in the case of the point charge. Noteworthy, the shortening of C_1C_2 reflects on $\Delta^{\ddagger}E_r$, which is 12.9 and 6.7 kcal/mol for **SH**$^+$ and **S**, respectively.

The last case of the series, **SAu**$^+$, is particular instructive. In this case, in addition to the electrostatic and donation effect, there is the presence of certain amount of back-donation from the metal. C_1C_2 and C_1O are 1.431 and 1.288 Å, respectively.

All these finding are readily explained by the presence of two components contributing to the shortening of these bonds that are acting in an opposite way: electrostatic effects and donation shortens C_1C_2 and C_1O, while back-donation lengthens these bonds. Coherently, C_1C_2 is longest in the presence of $[AuCO]^+$ (low back-donation) and it shortens as the back-donation increases.

Table S3. Geometrical parameters (in Å) of **S**, computed and estimated (est.) Au-C1 bond properties (in electrons) and P_{back} (%) for non-symmetric [LAu-**S**]$^{n+}$ complexes.

L	d_{C1C2}	d_{C2C3}	d_{C2C4}	d_{C3C4}	Δd	CT_{tot}	CT_{back} (est.)	P_{back}
JP	1.447	1.538	1.534	1.462	0.074	0.146	-0.169	26
IPr	1.450	1.554	1.553	1.473	0.080	0.127	-0.144	27
PPh_3	1.444	1.557	1.557	1.469	0.088	0.211	-0.110	20
PCy_3	1.446	1.556	1.554	1.471	0.084	0.187	-0.127	24
PAr^F	1.439	1.561	1.561	1.467	0.094	0.243	-0.085	14
$P(OMe)_3$	1.442	1.559	1.558	1.468	0.090	0.203	-0.102	18
$P(OPh)_3$	1.441	1.558	1.558	1.468	0.090	0.217	-0.102	18
ACPP	1.427	1.578	1.582	1.456	0.124	0.350	0.041	-12

Table S4. Geometrical parameters (in Å) of **S'**, computed and estimated (est.) Au-C1 bond properties (in electrons) and P_{back} (%) for non-symmetric [LAu-**S'**]$^{n+}$ complexes.

L	d_{C1C2}	d_{C2C3}	d_{C3C4}	Δd	CT_{back}	P_{back}
CO	1.401	1.608	1.440	0.168	-0.064	7
Cl^-	1.439	1.562	1.468	0.094	-0.292	48
CH_3O^-	1.449	1.554	1.475	0.079	-0.374	56
PPh_3	1.412	1.591	1.450	0.141	-0.136 [a]	22
IPr	1.419	1.581	1.454	0.127	-0.186 [a]	30
$P(OMe)_3$	1.409	1.594	1.447	0.147	-0.116 [a]	18
$P(OPh)_3$	1.409	1.593	1.448	0.146	-0.120[a]	19
NHC	1.415	1.588	1.451	0.137	-0.128	24

[a]Estimated value

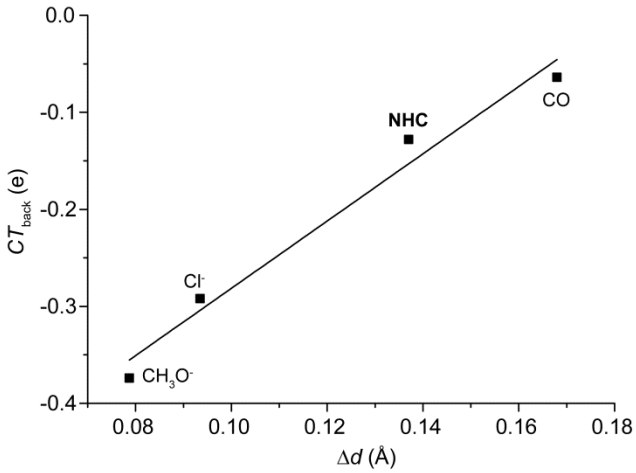

Figure S8. Linear correlations between Δd and CT_{back} for [LAu-**S'**] complexes.

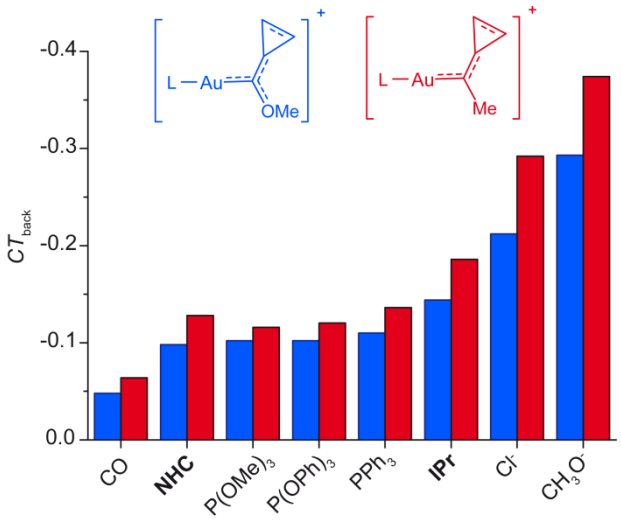

Figure S9. Correlation between the Au → C_1 back-donation in the case of **S** and **S'**.